

Wind-induced fragility assessment of urban trees with structural uncertainties

Yongbo Peng^{1,2a}, Zhiheng Wang^{3b} and Xiaoqiu Ai^{*2}

¹State Key Laboratory of Disaster Reduction in Civil Engineering, Tongji University, Shanghai 200092, China

²Shanghai Institute of Disaster Prevention and Relief, Tongji University, Shanghai 200092, China

³Department of Civil and Environmental Engineering, University of Southern California, Los Angeles, CA 90089, USA

(Received September 18, 2017, Revised December 7, 2017, Accepted December 9, 2017)

Abstract. Wind damage of urban trees arises to be a serious issue especially in the typhoon-prone areas. As a family of tree species widely-planted in Southeast China, the structural behaviors of Plane tree is investigated. In order to accommodate the complexities of tree morphology, a fractal theory based finite element modeling method is proposed. On-site measurement of Plane trees is performed for physical definition of structural parameters. It is revealed that modal frequencies of Plane trees distribute in a manner of grouped dense-frequencies; bending is the main mode of structural failure. In conjunction with the probability density evolution method, the fragility assessment of urban trees subjected to wind excitations is then proceeded. Numerical results indicate that small-size segments such as secondary branches feature a relatively higher failure risk in a low wind level, and a relatively lower failure risk in a high wind level owing to windward shrinks. Besides, the trunk of Plane tree is the segment most likely to be damaged than other segments in case of high winds. The failure position tends to occur at the connection between trunk and primary branches, where the logical protections and reinforcement measures can be implemented for mitigating the wind damage.

Keywords: finite element modeling; fractal theory; grouped dense-frequencies; fragility assessment; probability density evolution method; Plane tree

1. Introduction

Most of countries in the typhoon zones tend to suffer from huge economic losses in recent years. An eye-catching wind-disaster event, which was named the typhoon "Hagupit", occurred at China in 2008 that attacked the coastal areas of Guangdong Province and caused a serious economic loss over 13.4 billion RMB. Amongst these wind-induced economic losses, a large proportion were resulted from the damage of urban trees. It might be expected to increase due to the development of urbanization as well as due to climate change and extreme weather patterns predicted for the future. In August 1988, typhoon "8807" launched at Hangzhou, China, where thousands of urban trees were attacked, and 10.23% of urban trees was damaged resulting in that almost 80% of power transmission lines was broken in that area. In October 1999, typhoon "9914" launched at Xiamen, China, where 23 thousand trees were damaged coming 75% of urban trees. It is reported that over 20,000 trees were blown down in Shanghai, China in the period of 1951 to 2000, whereby more than 2,000 wire poles were broken causing the deaths of dozens of people. As a result, it is necessary to understand the dynamic behaviors and damage mechanism of urban trees induced by winds in order to provide a deep insight into mitigating wind disaster happened in urban

areas.

Over the past half century, a series of attempts have been made to study wind-induced failure of trees in the worldwide. Simplified models received great appeal in the early stage which relied upon static and dynamic equations involving a collection of critical parameters such as top displacement and stem bending moment of trunk (Baker 1995). These models can be classified into the experimental data-driven empirical model (Gardiner 1995, Gardiner *et al.* 2000), the theoretical model (Baker 1995, Saunderson 1999), and the mass-spring model (James 2006). Due to the limitations of prior hypothesis, however, the simplified model cannot meet the requirements of accuracy required to predict the tree damage. In recent years, the finite element method (FEM) has been proved to be valuable in wind-damage analysis of trees due to its versatility and compatibility (Sellier *et al.* 2008). Previous models for modal characteristics of Douglas fir (Moore and Maguire 2008), for mechanical response of maritime pine (Sellier and Fourcaud, 2009), for dynamic behaviors of maple (Ciftci *et al.* 2014), and for damage mechanism of Ginkgo (Ai *et al.* 2016) were implemented.

While the structural configuration of trees arises to be complicated, which significantly separates from the specimens though most of them consist of trunk, primary branches and secondary branches. Even for the same species, the sample configuration has a remarkable difference from others due to the growing conditions and man-made influences (Mattheck 1990). This brings about an extreme difficulty for the accurate modeling of wooded trees. Apart from the spatial configuration of trees, besides, the material parameters of wood act as the critical aspect as

*Corresponding author, Assistant Professor

E-mail: aixiaoqiu@tongji.edu.cn

^a Ph.D.

^b Ph.D. Candidate

well that influences the dynamic behaviors of tree samples (Cheng 1992). It is thus necessary to integrate the stochastic parameters representing the variation, respectively, from the spatial configuration and from the material characteristics into the finite element models. This treatment would provide a logical manner for the wind-induced fragility assessment of urban trees in the typhoon-prone areas. However, the previous efforts have not been paid on this issue.

In this study, the parametric modeling and stochastic dynamics analysis of urban trees are carried out. For illustrative purposes, the Plane tree, a family of tree species widely-planted in Southeast China, is investigated. Randomness inherent in the tree configuration and material characteristics is included in the modeling and dynamics analysis of urban trees. The sections arranged in this paper are distributed as follows. Section 2 is dedicated to illustrating the parametric model of Plane tree, including parameter definition, fractal theory based configuration and finite element model. The probabilistic analysis of dynamic behaviors of Plane tree is presented in Section 3. Section 4 details the stochastic dynamic response of Plane tree subjected to wind excitations. The concluding remarks are included in the final section.

2. Parametric model of Plane tree

The dynamic behaviors of urban trees seriously rely upon the species. Plane tree is the most used species in Shanghai, China. Fig. 1 shows the former ten species widely-planted in this area.

The Plane tree belongs to the *Platanus orientalis* Linn. It height could reach up to 30 meters. The benchmark configuration of the Plane tree submits to the Rauh's model (Halle *et al.* 1978, Tomlinson 1983, Prusinkiewicz and Rempfrey 2000). The basic configuration consists of the straight trunk, primary and secondary branches. The geometric shape arises to be of high symmetry. Although the parametric model of Plane tree could be proceeded as the benchmark, the accurate model is difficult since the Plane tree in reality arises to different poses due to the hybridization and trimming in the period of its growing. It is thus necessary to carry out a statistical analysis as to the specimens in order to implement the logical model of Plane trees.

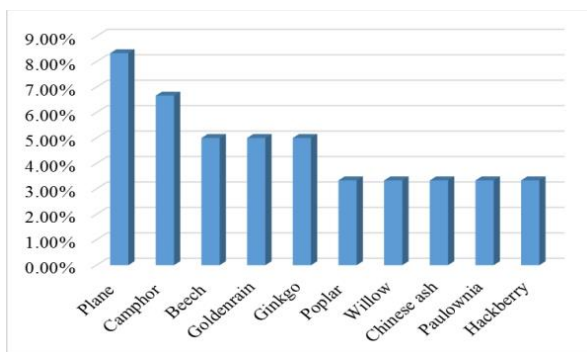


Fig. 1 The former ten species widely planted in Shanghai, China

2.1 Parameter definition

According to the survey of Plane trees planted along with Shanghai roads, the basic configuration with straight trunk like the benchmark is seldom. The trunk becomes to bifurcate usually at the elevation 2-3 m lift from the ground. The modes of bifurcation involve 2-primary branches, 3-primary branches and 4-primary branches. Among these modes, the 3-primary branches is at the most which occupies 60% of the Plane trees. In this paper, the 3-primary branches Plane tree is addressed.

Shown in Figs. 2 and 3 are the elevation view, projection view and geometric parameter label of a measured specimen of Plane trees, respectively. One might recognize that the basic geometric configuration of a Plane tree involves 14 parameters, i.e., the tree height H , trunk height h , stem perimeter of trunk d_b , top perimeter of trunk d_t , the measured separation h_0 between measured heights d_b and d_t , stem perimeter of primary branches $\{d_i\}_{i=1}^3$, projection angles between primary branches $\{\alpha_i\}_{i=1}^3$ ($\alpha_1 + \alpha_2 + \alpha_3 = 360^\circ$), projection angles between primary branches and trunk $\{\phi_i\}_{i=1}^3$. It is noted that using these geometric parameters, the basic configuration of Plane trees could be defined. While these parameters have an essential relationship so that the dimension of model parameters controlling the basic configuration could be reduced. Herein, the functional relationship between the stem perimeter of trunk and the tree height, the shrinkage rate of perimeter of trunk are addressed.



Fig. 2 Elevation view and geometric parameter label of a measured specimen of Plane trees

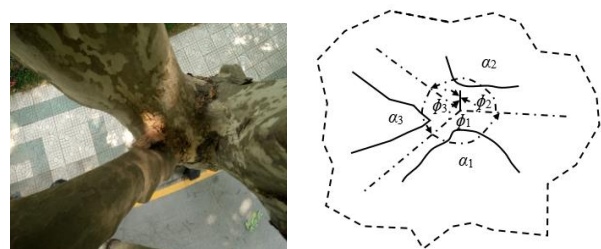


Fig. 3 Projection view and geometric parameter label of a measured specimen of Plane trees

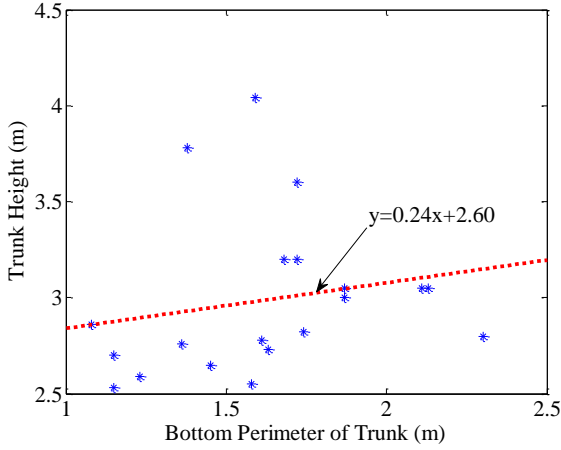


Fig. 4 Data points and fitting curve of trunk height against stem perimeter of trunk

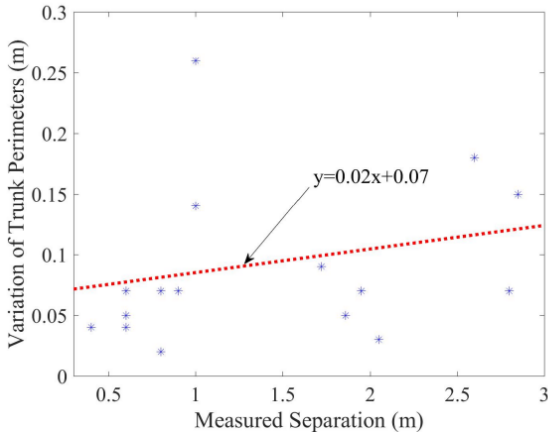


Fig. 5 Data points and fitting curve of variation of trunk perimeters against measured separations

More than 20 specimens of Plane trees are measured, and a collection of data is gained. Although the configuration of trees significantly relies upon the growing condition, there has a pertinent relevance of stem radius of trunk to the tree height for a certain species. It is usually recognized that owing to the natural law, the larger of radius of trunk, the taller of the tree arises to be. Fig. 4 shows the data points of the tree height against the stem perimeter of trunk. The functional curve fitting these data points is included as well. It is seen that there is a format of linear functional relationship between the tree height and the stem perimeter of the trunk.

The shrinkage rate of perimeter of trunk is formulated as well by fitting the data of relationship between variation of trunk perimeters and the length of measured heights (measured separation). It is shown in Fig. 5 that there is a linear functional relationship, and the slope denotes the shrinkage rate of perimeter of trunk.

The cross section of a trunk or a branch is identified by observing the tree samples, and is ideally assumed to be a solid circle. The cross-sectional area of the trunk is given by

$$A_i(z) = \pi[R(h_0)]^2 \quad (1)$$

where R is the radius of the trunk at height z , which is related to the stem perimeter by the equation as follows

$$R(h_0) = \frac{1}{2\pi}(d_b - \beta h_0) \quad (2)$$

where β is the shrinkage rate of perimeter of trunk. The radius of trunk R is the stem radius R_b at the measured separation $h_0 = 0$.

Assuming the branch has a same shrinkage rate of perimeter with that of the trunk, the radius of the branch is then given by

$$r(h_0) = \frac{1}{2\pi}(d_i - \beta h_0) \quad (3)$$

The ratio of the radius of the primary branches and the secondary branches is 0.5. It is indicated that the cross-section of both trunk and branches varies along the tree height.

2.2 Fractal theory based configuration

In view of the parameters defined in the previous section, one could implement the auto-generation of topology of trees. Two steps are usually involved: (i) define the basic configuration of trees that consists of trunk and primary branches; (ii) bifurcate the secondary branches at certain points on the primary branches. All the primary and secondary branches both submit to parabolic curves where the power exponents relevant to the primary branches and to the secondary branches are different but they have a pertinence. Treating the primary branches to the trunk and the secondary branches to the primary branches, the auto-generation of topology of trees can be implemented until the objective configuration is obtained through repeating the step (ii) in conjunction with the fractal theory.

The fractal theory reveals the resemblance between locality and totality of geometric object. This resemblance is the so-called self-similarity, which widely inhabits in the nature, such as the configuration of trees. If the self-similarity and scale invariance remain, the geometric object is a fractal structure. The locality could be viewed as a reduced-scale replication of totality. The mapping from the locality to the totality is referred to the affine transform.

The affine transform is essentially a linear transform. The angle between vectors, the distance from point to point and the area of graph might be changed. While the parallelity, intersection, collineation and symmetry would not be changed. The graph thus can be zoomed, stretched, trimmed and twisted. The formulation of affine transform is written by (Zhu and Ji 2011)

$$\begin{bmatrix} x' \\ y' \end{bmatrix} = \gamma \begin{bmatrix} \cos \theta & -\sin \theta \\ \sin \theta & \cos \theta \end{bmatrix} \begin{bmatrix} x \\ y \end{bmatrix} + \begin{bmatrix} e \\ f \end{bmatrix} \quad (4)$$

where x and y both denote the coordinates of graph before the transform; x' and y' are the projection of the original

coordinates x and y to the graph midpoint as a rule of affine transform; γ denotes the length coefficient of element; e and f denote the translational components of graph along x and y ; θ denotes the angle between the transformed figure and the original coordinate.

In this paper, the basic configuration of Plane tree consists of one trunk and three primary branches at the same elevation. The structural topology of Plane tree is formulated through the transform of the basic configuration at different heights of primary and secondary branches according to the auto-generation rules above mentioned. For simplified illustration, the second step of the auto-generation procedure is operated once. Nevertheless, two groups of secondary branches at different elevations are included. Three sets of secondary branches (9 secondary branches) at the same elevation are viewed as one group. It is seen from Fig. 6 that the secondary lower branches are labelled as Group 1; while secondary upper branches are labelled as Group 2. The control parameters of structural configuration involve the stem radius of trunk R_b , projection angles between primary branches $\{\alpha_1, \alpha_2\}$ ($\alpha_3 = 360^\circ - \alpha_1 - \alpha_2$), projection angles between primary branches and trunk $\{\phi_1, \phi_2, \phi_3\}$, shrinkage rate of radius β , angle between the transformed figure and the original coordinate θ . Fig. 6 shows the structural configuration of Plane tree with control parameters: $R_b = 0.25\text{m}$, $\alpha_1 = 112^\circ$, $\alpha_2 = 163^\circ$, $\phi_1 = 24^\circ$, $\phi_2 = 32^\circ$, $\phi_3 = 46^\circ$, $\beta = 0.02$, $\theta = 5^\circ$.

2.3 Finite element model

A mechanical model for finite element analysis is needed in order to assess the dynamic behaviors of Plane trees. While this is a challenging task due to the complex morphology of trees having a large number of branches and leaves. The dimensions and the shapes, moreover, of branches or leaves are significantly different from each other. It is neither feasible nor meaningful to measure the geometry of each branch accurately.

Owing to the introduction of configuration based on fractal theory, the geometric topology of model is readily defined. Furthermore, material of a real tree exposes to be composited, anisotropic, non-homogeneous, and elastoplastic. The component properties of trees not only vary along the dimensions, but also change across the sections. In this case, the material of the tree is assumed to be isotropic (the material properties are not dependent on the direction) and homogeneous (the material properties are the same at each point). The effects of the anisotropic and non-homogeneous are not taken into consideration. Thus, the wood density and Young's Modulus are considered to be a constant.

A three-dimensional beam element with circular cross section is used for modeling the tree, of which the beam axis is defined according to the tangent at the same location of the geometric model. Shear deformation effects are not included and behavior is described with the cross-sectional

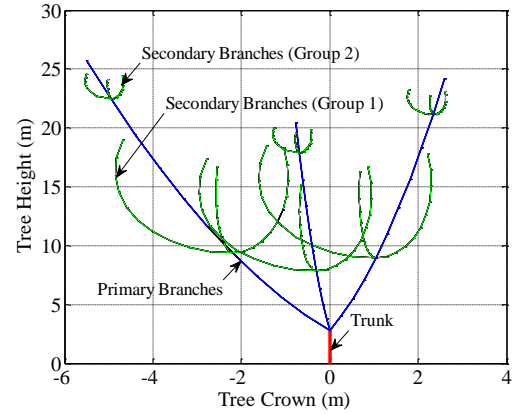


Fig. 6 Structural configuration of Plane tree with specified control parameters

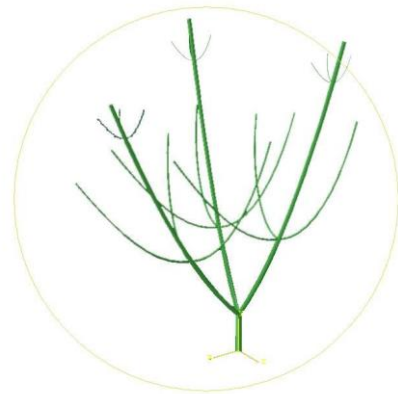


Fig. 7 Finite element model of Plane tree built up in ABAQUS

area and the isotropic, elastic-plastic material model.

A common MATLAB language program is produced to artificially mesh the geometric model of urban trees, and generate the ABAQUS input file. The trunk is divided into 10 elements. Each primary branch is divided into 10 elements and each secondary branch is divided into 10 elements. The total element numbers of the trunk, primary branches, and secondary branches, are thus to be 10, 30, and 180, respectively.

Boundary conditions for the model are treated as follows: the tree is clamped at its base, and rotation is fixed at each branching point (this is necessary for the branching points to support moments). The complete finite element model of tree is shown in Fig. 7. It is seen that the model is asymmetrical, close to the real configuration of Plane tree, and can be readily used to reveal the realistic dynamic behaviors of tree.

3. Probabilistic analysis of dynamic behaviors of Plane tree

3.1 Statistics and sampling of stochastic parameters

It is mentioned in the previous section that the control parameters of structural configuration involve the stem radius of trunk R_b , projection angles between primary branches $\{\alpha_1, \alpha_2\}$, projection angles between primary branches and trunk $\{\phi_1, \phi_2, \phi_3\}$. The shrinkage rate of radius β relies upon the tree species, and is valued by the statistical mean 0.02 referring to Fig. 5. The angle between the transformed figure and the original coordinate θ in the process of fractal-based structural configuration is defined by 5° . Fig. 8 shows the statistical histograms of the control parameters of structural configuration. It is seen that these parameters all arise to significant fluctuations. For a ready-modelling purpose, the priori distributions are assumed upon the control parameters in view of their histograms. The stem radius of trunk R_b , for instance, is assumed to submit to the log-normal distribution; the remaining 5 control parameters of structural configuration are assumed to submit to uniform distributions.

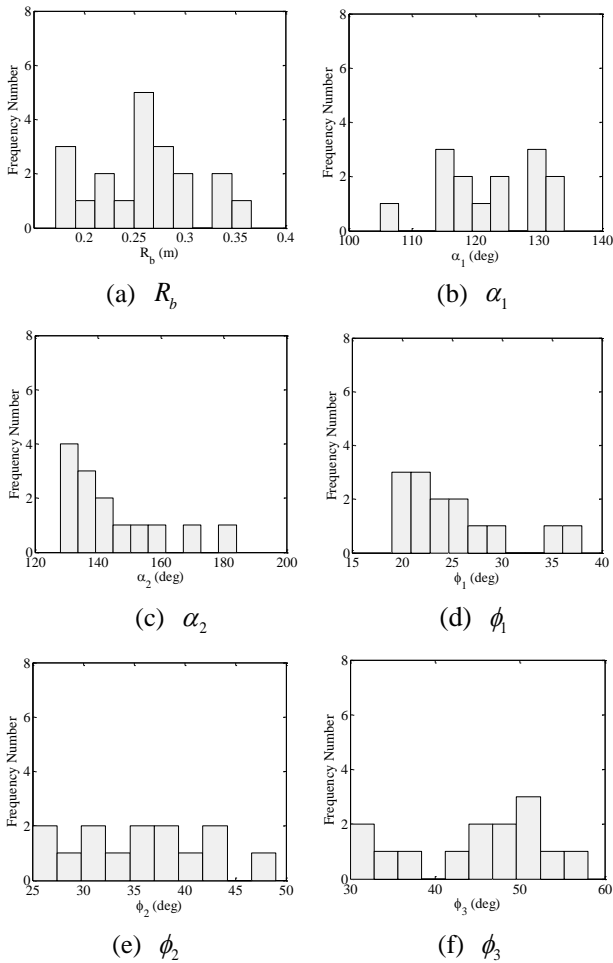


Fig. 8 Statistical histograms of the control parameters of structural configuration: (a) R_b , (b) α_1 , (c) α_2 , (d) ϕ_1 , (e) ϕ_2 and (f) ϕ_3

Table 1 Statistics and probability density function (PDF) of control parameters

Parameter/unit	PDF	Mean	Standard deviation
R_b /m	Log-Normal	0.2574	0.0538
α_1 /°	Uniform	117.42	16.76
α_2 /°	Uniform	153.86	30.6879
ϕ_1 /°	Uniform	25.36	5.88
ϕ_2 /°	Uniform	35.5	6.87
ϕ_3 /°	Uniform	44.71	8.62
E /Pa	Log-Normal	9.8×10^9	9.8×10^8
ρ /(g/cm ³)	Log-Normal	0.49	0.049

Besides, another two random parameters associated with the material behaviors of tree wood, i.e., wood air-dry density and Young's elastic modulus, are considered. They both are assumed to submit to the log-normal distribution. Therefore, there are formally 8 random variables underlying the parameters and configurations of Plane trees. The means and standard deviations of these variables are shown in Table 1, where the parameters of structural configuration are derived from the 20 sets of statistical data of on-site measurement of Plane trees; the parameters of structural material behaviors are referred to Reference (Prusinkiewicz and Remphrey 2000).

As to the sampling of high-dimensional systems with a collection of stochastic parameters, random simulation techniques are usually utilized. While a point set-optimization technique hinging upon the GF discrepancy is proved to be an efficient manner reducing computational costs and strengthening computational accuracy of nonlinear analysis and reliability assessment of stochastic structures (Chen and Zhang 2013). In this paper, the GF-discrepancy based sampling method is used to determine the point sets of the 8 random variables. Total 300 point sets are defined and each point set involves a group of sample values of the 8 random variables. The mean, standard deviation and PDF of random variables underlie these sample values.

3.2 Analysis of modal frequencies

Having the 300 point sets with sample values associated with random variables, one could construct the relevant 300 sample trees. In order to implement the finite element analysis by ABAQUS in loops, the values of control parameters of the sample trees are written into the individual inp. file. Utilizing the Python, one could code the inp. files into ABAQUS. Then the analysis of modal frequencies and stochastic dynamics of Plane trees can be readily proceeded.

The analysis of the oscillatory frequencies does not take mechanical loads into account, allowing for the model validation of Plane trees. Since the attenuating effect of the aerodynamic admittance function (Davenport 1961), i.e., there is a very little (less than 5%) energy transference to

plants by the modes above 5 Hz, the modal frequencies less than 5 Hz are extracted. Fig. 9 shows the distribution of the former 30-order modal frequencies of three sample trees, which covers a frequency range (0 Hz, 4.0 Hz]. In fact, over 90% of the wind energy is distributed in this frequency range. It is seen that owing to the randomness inherent in the material properties and structural topology, the modal frequencies of Plane trees change differently from the samples with respect to the modal number. The frequency variations along with samples and along with modes at the high-order modes both arise to be more pronounced than those at the low-order modes. One might recognize that these modes feature a remarkable pattern with grouped dense-frequencies, as indicated by the step dash-lines in Fig. 9. Among the former 30-order modal frequencies, the 1st and 2nd frequencies arise to bending modes of trunk (Trunk Bending); the 3rd to 6th frequencies correspond to bending modes of primary branches (Pri-Branch Bending); the 7th to 24th frequencies correspond to bending modes of secondary branches (Sec-Branch Bending); the remaining frequencies arise to torsional modes of trunk and branches (Torsional). Such a pattern with grouped dense-frequencies is consistent with the previous findings (James *et al.* 2006, Spatz *et al.* 2007).

One could further derive the probability density functions of modal frequencies at different modes through the kernel density estimation of the modal frequencies of all the sample trees. Fig. 10 shows the probability density functions of modal frequencies at the former 30-order modes. It is seen that consistent with the findings in Fig. 9, the frequency distribution at the high-order modes arise to be wider than that at the low-order modes, indicating a significant fluctuation of modal frequency at high-order modes due to the randomness inherent in the structural system of Plane trees. Moreover, the curves of probability density functions of modal frequencies at the same group of dense-frequencies, especially in case of the low modes, have an almost identical shape.

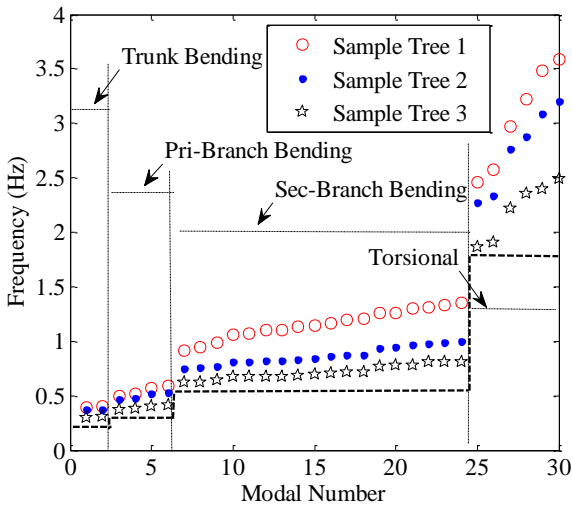


Fig. 9 Distribution of former 30-order modal frequencies of sample trees

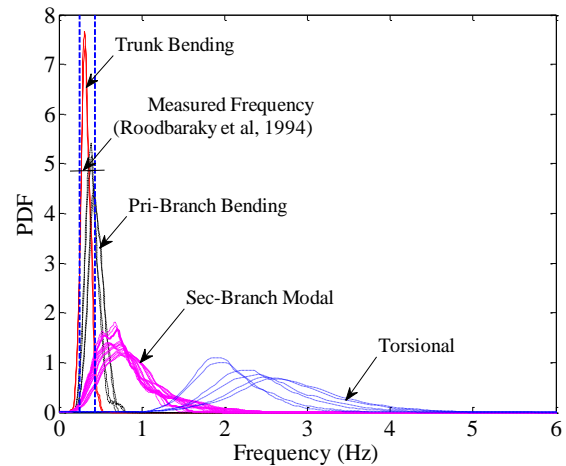


Fig. 10 Probability density functions of modal frequencies at former 30-order modes

It is indicated that the modal frequencies are not so sensitive to the randomness of the structural system in a same group of dense-frequencies. This is revealed in Fig. 11 as well, where the coefficients of variation associated with the groups of dense-frequencies Trunk Bending, Pri-Branch Bending, Sec-Branch Bending and Torsional are approximately 0.16, 0.20, 0.42, 0.23, respectively. One might realize that since the frequency range of bending modes corresponds to the most turbulent energy, the Plane tree mainly swaying as bending modes would have sound amplitude and variation of wind-induced vibration.

It is also indicated in Fig. 11 that the mean and standard deviation of the fundamental natural frequency of Plane trees by model prediction are 0.321 Hz and 0.051 Hz, respectively.

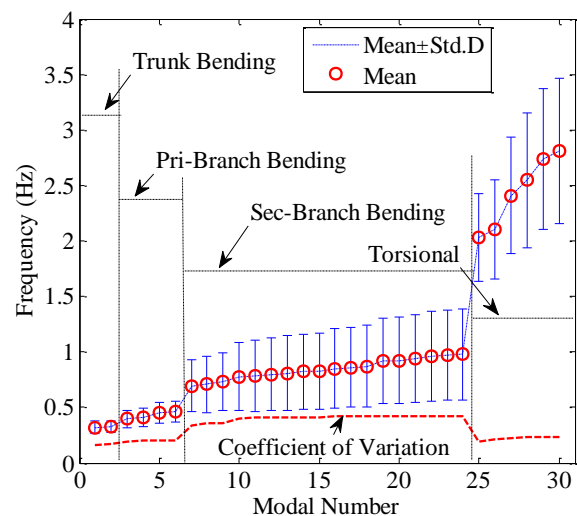


Fig. 11 Coefficients of variation associated with groups of dense-frequencies

A measurement of a small London Plane tree (*Platanus acerifolia*) from the power spectrum of tree displacement in winds shows that the natural frequency with summer in-leaf is at the range of 0.25-0.43 Hz (Roodbaraky *et al.* 1994). This result was later (after three years) proved to be in reasonably close agreement by measuring the power spectrum of velocity of the same tree using a tripod mounted Laser Doppler Interferometer (Baker 1997). This outcome provides a satisfactory check that the finite element model is logical and reasonable to examine the dynamic behavior of Plane trees.

4. Wind-induced failure criterion of Plane tree

It is noted in the previous sections that the Plane tree sways mainly as bending modes, indicating that the tree could be viewed to be damaged once the bending moment of an element in the model exceeds beyond its bending capacity. While this treatment would result in an issue of multiple failure modes due to the relevance among elements. Introducing the principle of equivalent extreme-value event (Li *et al.* 2007), the system reliability problem of multiple failure modes can be transformed into that of single failure mode.

Recognizing that the bending capacity and bending moment vary significantly with the elements, an indicative function of bending moment can be defined as

$$I_i(t) = \frac{M_i(t)}{\hat{M}_i}, \quad i = 1, 2, \dots, N_e \quad (5)$$

where $I_i(t)$ denotes the indicative function of bending moment; N_e denotes the total number of elements; $M_i(t)$ denotes the bending moment of the element i ; \hat{M}_i denotes the bending capacity of the element. $|I_i| > 1$ indicates the tree structure being broken; while $|I_i| \leq 1$ indicates the tree structure being safe.

The bending capacity of the element \hat{M}_i is calculated as followed

$$\hat{M}_i = \sigma_{\max} \cdot W_i \quad (6)$$

where W_i denotes the bending-resistant section modulus of the element i , $W_i = \pi D_i^3 / 32$, D_i denotes the section diameter of the element i ; σ_{\max} denotes the stress of section, which is obtained from the constitutive material law of wood, (Ai *et al.* 2016).

The component reliability upon level-crossing criterion involves the construction of extreme-value event of indicative function of bending moment at each element, which is typically defined as the maximum value over the duration of the indicative function of bending moment

$$I_i^{\text{comp}} = \max_{t \in [0, T]} [I_i(t)] \quad (7)$$

For the system reliability of a structural segment such as

trunk, primary branches or secondary branches (Groups 1 and 2), the equivalent extreme-value event of indicative functions of bending moment is defined as follows

$$I^{\text{sys}} = \max_{1 \leq i \leq N_e^s} \left\{ \max_{t \in [0, T]} [I_i(t)] \right\} \quad (8)$$

where N_e^s denotes the number of elements in one structural segment.

One might recognize that the global reliability is a further integration of the system reliability with respect to structural levels.

Since the wind-induced response of the tree structure involving randomness inherent in material properties and structural topology is essentially a stochastic time series, the indicative functions of bending moment defined in Eqs. (7) and (8) are random variables. Therefore, the failure probability of a structural element or a structural segment of Plane trees corresponds to the 1-crossing of the extreme-value event or equivalent extreme-value event of indicative function of bending moment. The failure probability of a structural segment, for instance, associated with equivalent extreme-value event I^{sys} is defined herein

$$P_f = 1 - R = 1 - \Pr\{I^{\text{sys}}(\Theta) \in \Omega_s\} \quad (9)$$

where $\Pr\{\cdot\}$ denotes the probability of random event; Θ is the random vector denoting the randomness inherent in material properties and structural topology; Ω_s denotes the safety domain $[0, 1]$; R denotes the system reliability as counterpart of failure probability.

The solution of failure probability of a structural segment could refer to the random simulation method such as Monte Carlo simulation and the estimation method of probability density function. While as to the accurate solution of small-size samples involved in this paper, the probability density evolution method is a ready-implement manner for the stochastic response analysis of structural systems (Li and Chen 2009, Li *et al.* 2012, Peng *et al.* 2014). It also underlies the structural reliability through constructing a random process

$$Z(\tau) = \phi(I^{\text{sys}}(\Theta), \tau) \quad (10)$$

that satisfies the boundary conditions as follows

$$Z(\tau)|_{\tau=0} = 0, \quad Z(\tau)|_{\tau=\tau_c} = I^{\text{sys}}(\Theta) \quad (11)$$

According to the principal of probability conservation, the extended physical stochastic system $\{Z, \Theta\}$ is governed by the generalized probability density evolution equation (Li and Chen 2008)

$$\frac{\partial p_{Z\Theta}(z, \Theta, \tau)}{\partial \tau} + \dot{\phi}(I^{\text{sys}}(\Theta), \tau) \frac{\partial p_{Z\Theta}(z, \Theta, \tau)}{\partial z} = 0 \quad (12)$$

where $\dot{\phi}(I^{\text{sys}}(\Theta), \tau)$ denotes the velocity of the constructed random process $\phi(I^{\text{sys}}(\Theta), \tau)$ at condition of $\{\Theta = \theta\}$.

The initial condition associated with the generalized probability density evolution equation is given by

$$p_{z\Theta}(z, \Theta, \tau)|_{\tau=0} = \delta(z - z_0)p_{\Theta}(\Theta) \quad (13)$$

The joint probability density function of $Z(\tau, \Theta)$ is then derived as $p_{z\Theta}(z, \Theta, \tau)$ by solving the generalized probability density evolution equation. The marginal probability density function $p_z(z, \tau)$ is then obtained through integration method

$$p_z(z, \tau) = \int_{\Omega_{\Theta}} p_{z\Theta}(z, \Theta, \tau) d\Theta \quad (14)$$

where Ω_{Θ} denotes the distribution domain of Θ .

In view of Eq. (11), the failure probability is thus obtained as the integration of the marginal probability density function $p_z(z, \tau)$ at the terminal instant

$$P_f = 1 - R = 1 - \int_{\Omega} p_z(z, \tau = \tau_c) dz \quad (15)$$

One might recognize that a critical step solving Eq. (15) is the definition of functional relationship $\phi(\cdot)$ between constructed random process $Z(\tau)$ and the indicative function $I^{\text{sys}}(\Theta)$. The functional relationship $\phi(\cdot)$ has really variant formulations satisfying the boundary conditions; say Eq. (11). A ready formulation is built in the harmonic function as follows

$$Z(\tau) = \phi(I^{\text{sys}}(\Theta), \tau) = I^{\text{sys}}(\Theta) \sin(\omega\tau) \quad (16)$$

where $\omega = 2.5\pi$, $\tau_c = 1$. It is really proved that Eq. (16) satisfies the requirements of Eq. (11).

5. Wind-induced fragility assessment of Plane tree

The equation of swaying motion of tree structure subjected to wind loading reads

$$\mathbf{M}(\Theta)\ddot{\mathbf{X}}(t) + \mathbf{C}(\Theta)\dot{\mathbf{X}}(t) + \mathbf{f}[\mathbf{X}(\Theta, t)] = \mathbf{F}(t) \quad (17)$$

where \mathbf{M} and \mathbf{C} denote the mass and damping matrices of the, respectively; $\ddot{\mathbf{X}}(t)$, $\dot{\mathbf{X}}(t)$, $\mathbf{X}(t)$ denote vectors of the acceleration, velocity, and displacement of the tree with respect to ground, respectively; $\mathbf{f}[\mathbf{X}(\Theta, t)]$ denotes a vector of internal restoring forces, serving as a function of the elemental deflections; The swaying motion of trees subjected to wind actions involves geometric nonlinearity and material nonlinearity, of which the nonlinear effect is included in the term of restoring forces $\mathbf{f}[\mathbf{X}(\Theta, t)]$ that might result in the challenge of computational efforts (Li *et al.* 2011); Rayleigh damping is used to approximate the damping matrix $\mathbf{C} = k_1\mathbf{M} + k_2\mathbf{K}$, where k_1 and k_2 are Rayleigh damping factors relying upon the modal frequencies and damping ratios; $\mathbf{F}(t)$ denotes the vector of the time-dependent wind loading.

The logical definition of wind loading upon a tree is a challenging issue due to the complexity inherent in the flow and turbulence structures around the tree (Aung *et al.* 2012, Aly *et al.* 2013, Lee *et al.* 2014). In this paper, the

interaction between the wind and the tree is treated as a wind drag force (Ciftci *et al.* 2014), which is modelled as a distributed line loads acting on the finite element model in x direction (all loadings are applied in a horizontal direction).

The drag force acting on the element i is expressed as

$$F_i(t) = 0.5\rho_a A_i(t) C_D U_i^2(t) \quad (18)$$

where $U_i(t)$ denotes the wind speed distributing on the element; $A_i(t)$ denotes the project area of the element, which is time-dependent quantity due to a significant influence of elemental deflections upon the project area; ρ_a denotes the density of air; C_D denotes the drag coefficient. The density of air and the drag coefficient are assumed to be 1.2 kg/m^3 and 0.47 , respectively (Rudnicki *et al.* 2004).

The wind speed process $U_i(t)$ at a height includes two components: the time-averaged component \bar{U}_i and the fluctuating component $u_i(t)$ (Dyrbye and Hansen 1997). The time-averaged component $\bar{U}(z_i)$ could be represented by an exponential-type function relevant to the height (Ciftci *et al.* 2014). While the fluctuating component $u_i(t)$ is typically reviewed as a zero-mean Gaussian process (Kareem 2008, Li *et al.* 2013), so that all of the properties can be completely reflected by a pertinent power spectral density function. For the structure of Plane tree, it is necessary to reflect mutual relations among fluctuating wind speeds in different positions of space because of its large volume. At this point, the spatial fluctuating wind speed is a time-varying stochastic field. Thus, the fluctuating component $u_i(t)$ depends on the spatial coordinates of elements as well as on the time t .

The relationship between fluctuating wind speeds at two points of space can be determined by complex cross-power spectral density function $S_{u_i u_j}(\omega)$

$$S_{u_i u_j}(\omega) = \gamma_{ij}(\Delta y, \Delta z, \omega) \sqrt{S_{u_i u_i}(\omega) S_{u_j u_j}(\omega)} \quad (19)$$

where $\gamma_{ij}(\Delta y, \Delta z, \omega)$ is the so-called coherence function with respect to lateral and vertical separations, in the form of Eq. (20)

$$\gamma_{ij}(\Delta y, \Delta z, \omega) = \exp(-f_{ij}(\omega)) \quad (20a)$$

$$f_{ij}(\omega) = \frac{|\omega| \sqrt{C_y^2 (y_j - y_i)^2 + C_z^2 (z_j - z_i)^2}}{\pi [\bar{U}(z_j) + \bar{U}(z_i)]} \quad (20b)$$

where C_y and C_z denote decay coefficients of the lateral and vertical coherences, respectively (Yan *et al.* 2013, Peng *et al.* 2018); ω denotes the circular frequency.

A commonly-used downwind pulsation wind speed spectrum irrelevant to altitude is employed herein (Davenport 1961)

$$S_{u_i}(\omega) = \frac{1}{2} \frac{4u_s f^2}{\omega(1+f^2)^{4/3}} \quad (20a)$$

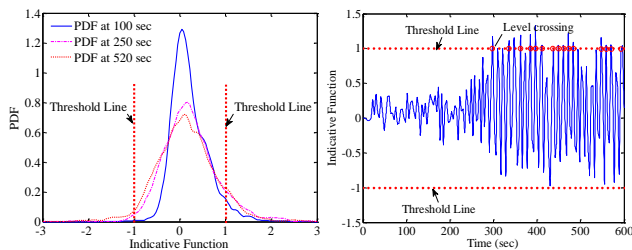
$$f = \frac{1200\omega}{2\pi\bar{U}_0} \quad (20b)$$

where \bar{U}_0 denotes the average wind speed at height 10 m; u_s denotes the shear wave speed.

In view of spectral representation method for simulation of one-dimensional multivariable stationary random process (Shinozuka and Jan 1972, Deodatis 1996, Shinozuka and Deodatis 1997, Liu *et al.* 2016, Liu *et al.* 2018), the stochastic wind fields can be simulated at different wind levels represented by average wind speeds (average wind speeds at height of 10 m are 12, 16, 20, 24, 28 and 32 m/s, respectively). At each wind level, the time history of wind speed is obtained at the height of the element of Plane tree specimens. Total 220 time histories, for a Plane tree specimen, of wind loadings acting at 220 elements are involved.

Utilizing the probability density evolution method, stochastic dynamic response analysis of Plane tree systems under six wind levels is performed. Time-history integration techniques for deterministic dynamic analysis of samples and finite difference methods for solving the generalized probability density evolution equation are involved. In this study, the time length of wind loading process is defined to be 600 sec, and the time step in simulation of wind field is 0.25 sec. While the time step in numerical integration by ABAQUS varies with time process as a certain criterion. In conjunction with the sampling of high-dimensional systems and point set-optimization, the 300 samples of Plane tree with the assigned probabilities are integrated for probabilistic illustration.

Fig. 12(a) shows the indicative function of bending moment at the 10th element of Plane tree (an element of trunk) with respect to the probability density curves at typical instants of time 100 sec, 250 sec, 520 sec.



(a) probability density curves at typical instants of time

(b) sample process

Fig. 12 Indicative function of bending moment of an element of Plane tree in case of average wind speed 24 m/s as to: (a) probability density curves at typical instants of time and (b) sample process

It is revealed that the probability density curve of indicative function of bending moment changes with the instants of time, which has an indistinctive fluctuation during the first 100 sec while its variation becomes significant in the remaining time interval. The domain, as shown between the double-threshold lines, indicates a safe state of Plane tree; while the domain beyond the threshold lines indicates a failure state of Plane tree. This provides a foundation for probability-based risk analysis of Plane trees subjected to wind hazard. For a straightforward illustration, a sample process of the indicative function of bending moment at the 10th element of Plane tree in case of average wind speed 24 m/s is shown in Fig. 12(b). It is seen that the population associated with the probability density function have similar properties to the sample. One might realize as well that the failure of Plane tree is a frequently-occurring event in case of the wind level with average wind speed 24 m/s since there is a low component reliability (less than 0.8) occurring on the element of trunk. The addressed 10th element is just the branch-off position of trunk that is proved to be the most likely damaged element in the following text.

Extending the above-mentioned to the system reliability and all the cases of wind levels, the fragility assessment of segments of Plane tree could be proceeded (Ellingwood and Rosowsky 2004). Fig. 13 shows the fragility curves of the segments of Plane tree subjected to variant wind levels with average wind speeds from 12 m/s to 32 m/s. It is seen that in case of average wind speed less than 18 m/s, if an interpolation of failure probability is accepted, the secondary lower branches (Group 1) has a larger failure risk, and the failure probability of segments rank as secondary lower branches > trunk > primary branches > secondary upper branches. While in case of average wind speeds between 18 m/s and 20 m/s, the trunk has a larger failure risk, and the failure probability of segments rank as trunk > secondary lower branches > primary branches > secondary upper branches. In case of average wind speeds between 20 m/s and 32 m/s, the trunk still has a larger failure risk, and the failure probability of segments rank as trunk > primary branches > secondary lower branches > secondary upper branches. The secondary upper branches (Group 2) always has a lower failure risk through the wind levels. One might recognize that the numerical results have the logical reason: failure probability of bending moment of structural segments relies both upon their bending capacities and moment response; the segment has a smaller section indicating a lower bending capacities but a lower moment response since the loading force on the segment is smaller.

In general, the loading force on a small-size segment is pronounced due to a small deflection in case of a low wind level, whereby a larger failure risk than other big-size segments is recognized. When the wind level increases, small-size segments sway significantly and gain a slow enhancement of moment response owing to windward shrinks; while the wind effect upon the large-size segments increases dramatically owing to the square relationship between wind pressure and wind speed, and an almost invariant windward since an adequate stiffness of the large-

size segments, which results in a quick enhancement of moment response.

It is also indicated that the failure of Plane tree is a low-probability event (failure probability is almost 0.9) since all the segments of tree have a small failure probability in case of the wind level with average wind speed less than 20 m/s; while the failure of Plane tree increases significantly in case of the wind level with average wind speed more than 20 m/s. The wind speed 20 m/s is thus defined as the failure wind speed of Plane tree, which serves as one of critical wind speeds associated with the wind-resistant capacity of trees (Virot *et al.* 2016).

It is seen that in case of high winds, the trunk of Plane tree is the segment most likely to be damaged than other segments. For the practical protection of wind-induced vibration, a detail on the trunk position, of which the element might be broken prior to other elements, is needed. Thus, the indicative function of bending moment of trunk elements (element No. 1 to 10) is analyzed, i.e. how is the distribution of these samples of extreme-value events on the trunk elements. Fig. 14 shows the extreme value of indicative function I_i^{comp} distributed on the element numbers in different wind levels as the histogram of samples, i.e., the frequency number of I_i^{comp} occurring on a certain element through all the samples at a wind level. Wind level in the figure labelled by 1, 2, 3, 4, 5, 6 refers to the average wind speed 12 m/s, 16 m/s, 20 m/s, 24 m/s, 28 m/s and 32 m/s, respectively. It is readily revealed that the 10th element has the largest frequency number of I_i^{comp} throughout all the samples in case of different wind levels, indicating that the 10th element is the main contributor to the failure of trunk system, and the position of most likely failure occurs at the connection between trunk and primary branches. The branch-off element and its adjacent elements of trunk is thus the critical position where the logical protection and reinforcement measure are implemented; see Fig. 15.

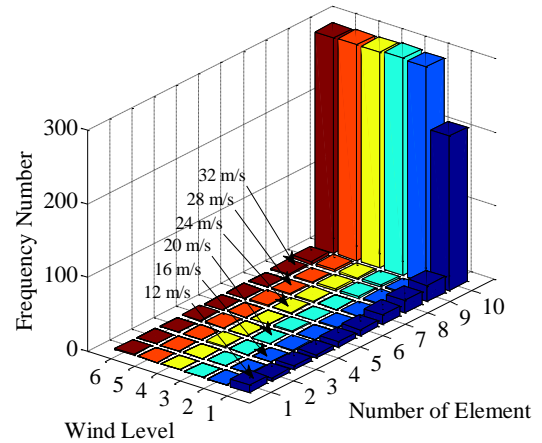


Fig. 14 Extreme value of indicative function distributed on element numbers in different wind levels as histogram of samples



Fig. 15 Protection and reinforcement measure implemented on trunk of Plane trees

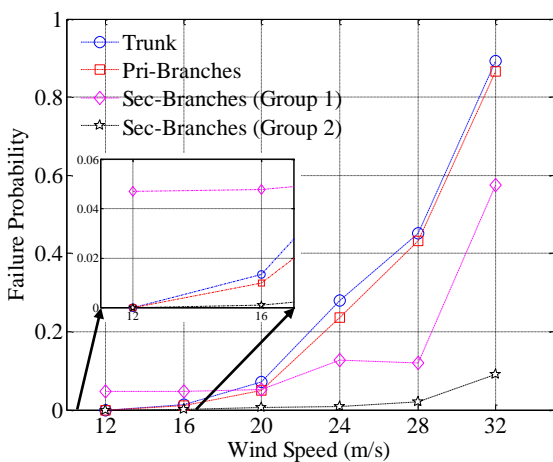


Fig. 13 Fragility curves of the segments of Plane tree subjected to variant wind levels with average wind speeds from 12 m/s to 32 m/s

6. Conclusions

This paper is devoted to the parametric modeling and wind-induced fragility assessment of Plane trees, a family of widely-planted tree species in the area of Shanghai China, involving the randomness inherent in material properties and structural topology. A new technique of topology modeling of tree structures integrating the fractal theory and the finite element method is proposed. Fragility probability analysis of Plane trees subjected to wind hazard then receives a significant breakthrough utilizing the probability density evolution method. This has a certain engineering application value and the practical significance in risk assessment of urban trees. The main conclusions are summarized as follows.

- Fractal theory based modeling of structural topology accommodates the complexities of Plane tree morphology. Kernel parameters involved in the model reveals the variation of structural morphology and material properties,

which are identified and statistically analyzed from the measurement data of Plane trees. This treatment overcomes the non-logics associated with traditional models through considering the uncertainty inherent in tree morphology and biomechanics due to growing conditions. The logical model underlies the investigation of structural dynamics of Plane trees and wind-induced risk assessment at an individual-tree or at a block-trees scales.

- The mean and standard deviation fundamental natural frequency of Plane trees by model prediction are 0.321 Hz and 0.051 Hz, respectively, which shows a consistence with the previous measurements of London Plane trees. The modal frequencies of sample trees feature a remarkable pattern with grouped dense-frequencies. Among the former 30-order modal frequencies, the 1st and 2nd frequencies correspond to bending modes of trunk; the 3rd to 6th frequencies correspond to bending modes of primary branches; the 7th to 24th frequencies correspond to bending modes of secondary branches; the remaining frequencies correspond to torsional modes of trunk and branches. The statistical analysis of modal frequencies indicates that the bending mode is the main manner of structural failure of Plane trees.

- Failure probability of bending moment of structural segments relies both upon their bending capacities and moment response. In case of a low wind level, the loading force on a small-size segment such as the secondary branches is pronounced due to a small deflection, which results in a larger moment response and a higher failure risk than other big-size segments, i.e., the trunk. With the increasing of the wind level, small-size segments sway significantly and gain a slow enhancement of moment response owing to windward shrinks; while the wind effect upon the large-size segments increases dramatically since there is an almost invariant windward since an adequate stiffness of the large-size segments.

- In case of high winds, the trunk of Plane tree is the segment most likely to be damaged than other segments. The element closing to the branch-off point between the trunk and the primary branches is the main contributor to the failure of trunk system. The position of most likely failure thus occurs at the connection between trunk and primary branches, where the logical protections and reinforcement measures can be implemented for mitigating the damage caused by wind-induced vibration.

Acknowledgments

The supports of the National Key R&D Program of China (Grant No. 2017YFC0803300), the Ministry of Science and Technology of China (Grant Nos. SLDRCE13-MB-04 & SLDRCE14-B-20), and the Fundamental Research Funds for the Central Universities of China are highly appreciated. Prof. Jie Li is greatly appreciated for his constructive discussions and comments on the research.

References

- Ai, X., Cheng, Y. and Peng, Y.B. (2016), "Nonlinear dynamics and failure wind velocity analysis of urban trees", *Wind Struct.*, **22**(1), 89-106.
- Aly, A.M., Fossati, F., Muggiasca, S., Argentini, T., Bitsuamlak, G., Franchi, A. and Chowdhury, A.G. (2013), "Wind loading on trees integrated with a building envelope", *Wind Struct.*, **17**(1), 69-85.
- Aung, N.N., Ye, J. and Masters, F.J. (2012), "Simulation of multivariate non-Gaussian wind pressure on spherical latticed structures", *Wind Struct.*, **15**(3), 223-245.
- Baker, C.J. (1995), "The development of a theoretical model for the windthrow of plants", *J. Theor. Biol.*, **175**(3), 355-372.
- Baker, C.J. (1997), "Measurements of the natural frequencies of trees", *J. Exper. Botany*, **48**(5), 1125-1132.
- Chen, J.B. and Zhang, S.H. (2013), "Improving point selection in cubature by a new discrepancy", *SIAM J. Scientific Comput.*, **35**(5), 2121-2149.
- Cheng, J. (1992), *China Wood Journal*, China Forestry Publishing House, Beijing, China.
- Ciftci, C., Arwade, S.R., Kane, B. and Brena, S.F. (2014), "Analysis of the probability of failure for open-grown trees during wind storms", *Probabilist. Eng. Mech.*, **37**, 41-50.
- Davenport, A.G. (1961), "The spectrum of horizontal gustiness near the ground in high winds", *Q. R. J. Meteor. Soc.*, **87**(372), 194-211.
- Deodatis, G. (1996), "Simulation of ergodic multivariate stochastic processes", *J. Eng. Mech. -ASCE*, **122**(8), 778-787.
- Dyrbye, C. and Hansen, S.O. (1997), *Wind Loads on Structures*, John Wiley & Sons, New York, USA.
- Ellingwood, B.R. and Rosowsky, D.V. (2004), "Fragility assessment of structural systems in light-frame residential construction subjected to natural hazards", *In Structures 2004: Building on the Past, Securing the Future*, 1-6.
- Gardiner, B.A. (1995), "The interactions of wind and tree movement in forest canopies", (Eds., Coutts, M.P. and Grace, J.), *Wind Trees*, 41-59, Cambridge: Cambridge University Press.
- Gardiner, B.A., Peltola, H. and Kellomaki S. (2000), "Comparison of two models for predicting the critical wind speeds required to damage coniferous trees", *Ecol. Model.*, **129** (1), 1-23.
- Halle, F. Oldeman, R.A.A. and Tomlinson, P.B. (1978), *Tropical Trees and Forests: An Architectural Analysis*, New York: Springer-Verlag.
- James, K.R., Haritos, N. and Ades, P.K. (2006), "Mechanical stability of trees under dynamic load", *Am. J. Botany*, **93**(10), 1522-1530.
- Kareem, A. (2008), "Numerical simulation of wind effects: a probabilistic perspective", *J. Wind Eng. Ind. Aerod.*, **96**(10), 1472-1497.
- Lee, J.P., Lee, E.J. and Lee, S.J. (2014), "Effect of trunk length on the flow around a fir tree", *Wind Struct.*, **18**(1), 69-82.
- Li, J. and Chen, J.B. (2008), "The principle of preservation of probability and the generalized density evolution equation", *Struct. Saf.*, **30**(1), 65-77.
- Li, J., Chen, J.B., Sun, W.L. and Peng, Y.B. (2012), "Advances of the probability density evolution method for nonlinear stochastic systems", *Probabilist. Eng. Mech.*, **28**, 132-142.
- Li, J., Peng, Y.B. and Chen, J.B. (2011), "Nonlinear stochastic optimal control strategy of hysteretic structures", *Struct. Eng. Mech.*, **38**(1), 39-63.
- Li, J. and Chen, J.B. (2009), *Stochastic Dynamics of Structures*, Wiley, New York, USA.
- Li, J., Chen, J.B. and Fan, W.L. (2007), "The equivalent extreme-value event and evaluation of the structural system reliability", *Struct. Saf.*, **29**(2), 112-131.
- Li, J., Peng, Y.B. and Yan, Q. (2013), "Modeling and simulation of

- fluctuating wind speeds using evolutionary phase spectrum”, *Probabilist. Eng. Mech.*, **32**, 48-55.
- Liu, Z.J., Liu, W. and Peng, Y.B. (2016), “Random function based spectral representation of stationary and non-stationary random processes”, *Probabilist. Eng. Mech.*, **45**, 115-126.
- Liu, Z.J., Liu, Z.H. and Peng, Y.B. (2018), “Simulation of multivariate stationary stochastic processes using dimension-reduction representation methods”, *J. Sound Vib.*, **418**, 144-162.
- Mattheck, C. (1990). “Why they grow, how they grow: The mechanics of trees”, *Arboricultural J.*, **14**(1), 1-17.
- Moore, J.R. and Maguire, D.A. (2008), “Simulating the dynamic behavior of Douglas-fir trees under applied loads by the finite element method”, *Tree Physiol*, **28**(1), 75-83.
- Peng, Y.B., Chen, J.B. and Li, J. (2014), “Nonlinear response of structures subjected to stochastic excitations via probability density evolution method”, *Adv. Struct. Eng.*, **17**(6), 801-816
- Peng, Y.B., Wang, S.F. and Li J. (2018), “Field measurement and investigation of spatial coherence for near-ground strong winds in southeast China”, *J. Wind Eng. Ind. Aerod.*, **172**, 423-440.
- Prusinkiewicz, P. and Remphrey, W.R. (2000), “Characterization of architectural tree models using L-systems and Petri nets”, *L'arbre – the Tree*, 177-186.
- Roodbaraky, H.J., Baker, C.J., Dawson, A.R. and Wright, C.J. (1994), “Experimental observations of the aerodynamic characteristics of urban trees”, *J. Wind Eng. Ind. Aerod.*, **52**, 171-184.
- Rudnicki, M., Mitchell, S.J. and Novak, M.D. (2004), “Wind tunnel measurements of crown streamlining and drag relationships for three conifer species”, *Can. J. Forest Res.*, **34**(3), 666-676.
- Saunderson, S.E.T., Baker, C.J. and England, A. (1999), “A dynamic model of the behaviour of Sitka Spruce in high winds”, *J. Theor. Biol.*, **200**, 249-259.
- Sellier, D. and Fourcaud, T. (2009), “Crown structure and wood properties: Influence on tree sway and response to high winds”, *Am. J. Botany*, **96**(5), 885-896.
- Sellier, D., Brunet, Y. and Fourcaud, T. (2008), “A numerical model of tree aerodynamic response to a turbulent airflow”, *Forestry*, **81**(3), 279-297.
- Shinozuka, M. and Deodatis, G. (1997), “Simulation of stochastic processes and fields”, *Probabilist. Eng. Mech.*, **14**, 203-207.
- Shinozuka, M. and Jan, C.M. (1972), “Digital simulation of random processes and its applications”, *J. Sound Vib.*, **25**(1), 111-128.
- Spatz, H.C., Bruchert, F. and Pfisterer, J. (2007), “Multiple resonance damping or how do trees escape dangerously large oscillations?”, *Am. J. Botany*, **94**(10), 1603-1611.
- Tomlinson, P.B. (1983), “Tree architecture: new approaches help to define the elusive biological property of tree form”, *Am. Scientist*, **71**(2), 141-149.
- Virost, E., Ponomarenko, A., Dehandschoewercker, E., Quere, D. and Clanet, C. (2016), “Critical wind speed at which trees break”, *Phys. Rev. E*, **93**(2), 023001.
- Yan, Q., Peng, Y.B. and Li, J. (2013), “Scheme and application of phase delay spectrum towards spatial stochastic wind fields”, *Wind Struct.*, **16**(5), 433-455.
- Zhu, H. and Ji, C. (2011), *Fractal Theory and Its Application*, Science Press, Beijing, China. [in Chinese]